BNL-102222-2014-TECH
RHIC/AP/114;BNL-102222-2013-IR

Four Really Large Hadron Collider papers contributed to Snowmass 96

G. F. Dell

October 1996

Collider Accelerator Department
Brookhaven National Laboratory

U.S. Department of Energy
USDOE Office of Science (SC)

DISCLAIMER

RHIC/AP/114
October 1996

Four Really Large Hadron Collider papers contributed to Snowmass 96

F. Dell, M. Harrison, S. Peggs, M. Syphers, S. Tepikian, J. Wei,
Brookhaven National Laboratory
G. Goderre, Fermi National Accelerator Laboratory

This note acts as a preprint for the 4 papers that have been submitted to the proceedings of Snowmass 96 with authors "Peggs et al" and "Wei et al". Attached to this cover sheet are the following papers:

1. *Crab Crossing in a Large Hadron Collider*, J. Wei
2. *Interaction Region Analysis for a High-Field Hadron Collider*, J. Wei, G. Goderre, S. Peggs
3. *Lattices for a High-Field 30 TeV Hadron Collider*, S. Peggs, F. Dell, M. Harrison, M. Syphers, S. Tepikian
4. *Tolerable Systematic Errors in Really Large Hadron Collider Dipoles.* S. Peggs, F. Dell

Enjoy.

CRAB CROSSING IN A LARGE HADRON COLLIDER

Jie Wei
Brookhaven National Laboratory, Upton, New York 11973, USA

ABSTRACT

Since its invention by Palmer[1] in 1988, crab crossing has been explored by many people for both linear and storage ring colliders to allow for an angle crossing without a loss of luminosity. Various crab crossing scenarios have been incorporated in the design of newly proposed linear colliders and B-factory projects. For a hadron collider, this scheme can also be employed to lower β^* at the interaction point for a higher luminosity.

In this paper, we first review the principle and operational requirements of various crab crossing schemes for storage ring colliders. A Hamiltonian formalism is developed to study the dynamics of crab crossing and the related synchro-betatron coupling. Requirements are obtained for the operational voltage and frequency of the crab cavities, and for the accuracy of voltage matching and phase matching of the cavities.

For the recently proposed high-field hadron collider,[2, 3] a deflection crabbing scheme can be used to reduce β^* from 0.1 m to 0.05 m and below, without a loss of luminosity due to angle crossing. The required voltage of the storage rf system is reduced from 100 MV to below 10 MV. With the same frequency of 379 MHz operating in a transverse mode, the required voltage of the crab cavities is about 3.2~4.4 MV. The required accuracy of voltage and betatron-phase matching is about 1%.

I. INTRODUCTION

The subject of angle crossing at the interaction point (IP) of a storage ring collider has been studied for many years with the realization that the synchro-betatron resonance induced by the crossing angle severely limits the luminosity. In 1988, a beam-beam collision scheme was invented by Palmer[1]to allow a large crossing angle for a linear collider without a loss of luminosity. The Palmer scheme (or deflection crabbing scheme) employs transverse rf deflectors placed at locations where the betatron phase advance is $-90°$ from the IP. Both colliding bunches are tilted by the cavities by half the crossing angle at the IP so that they collide head-on. Subsequently, several alternative schemes[4, 5, 6, 7] were also introduced to apply crab crossing to storage ring colliders. Recently, various crab crossing scenarios have been incorporated in the design of newly proposed linear colliders[8] and B-factory projects.[9]

The design goal of a high-field hadron collider[2, 3, 10] is a 50 TeV storage ring that can achieve a peak luminosity of 10^{34} cm^{-2}·s^{-1} with a small number of interactions per bunch-bunch collision. With an experimental drift space of $\pm$25 m and a focusing strength of 360 T/m at the triplet quadrupoles, a β^* of 0.1 m can be achieved at the energy of 50 TeV. To enjoy the benefits of a relatively small bunch spacing, the beams must cross at an angle α of about 70μr to avoid more than one bunch-bunch collision in each experimental straight section. Such a non-zero crossing angle causes a degradation in luminosity. Consequently, it demands a short bunch length ($\sigma \approx 2$ cm) which can only be achieved with a large rf voltage (100 MV) when operating at a frequency of 379 MHz. The problem can be solved by crab crossing the two counter-circulating proton beams to make them collide head-on.

In Section II of this paper, we first summarize the principle and operational requirements of three crabbing schemes for storage ring colliders. A Hamiltonian formalism is developed in Section III to calculate the emittance growth and crabbing quality degradation produced by the errors in voltage and betatron-phase matching of the crab cavities. The results are applied to a conceptual design of angle crossing in the proposed high-field hadron collider. Conclusions and a discussion are given in Section IV.

II. CRAB CROSSING SCHEMES

The goal of crab crossing in a storage ring collider is to make the two counter-circulating angle-crossing beams collide head-on at the IP without sacrificing beam quality and luminosity lifetime. In this section, we present three schemes: deflection crabbing,[1] dispersive crabbing,[4] and η^* crabbing.[5] The angle crossing is assumed to occur in the horizontal (x–z) plane.

A. Deflection Crabbing

With the deflection crabbing scheme, as shown in Fig. 1, two transverse deflectors (rf cavities operating at their transverse

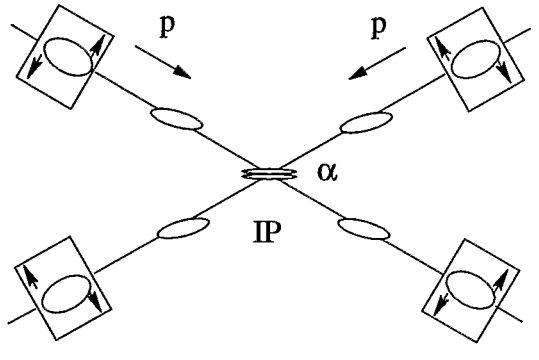

Figure 1: Schematic view of deflection crab crossing of two counter-circulating beams. The crossing angle between the two beam trajectories is α.

modes) are positioned on each side of the IP, preferably at high-β locations with betatron phase advances of $\pm 90°$ from the IP. At an azimuthal location s_0 with a betatron phase of $-90°$ from the IP, the particle receives a kick in the horizontal direction x, along with a change in momentum ($\delta \equiv \Delta p/p$),

$$\begin{aligned} \Delta x' &= \frac{K_0 R}{h_c} \sin\left(\frac{h_c}{R} z\right), \\ \Delta \delta &= K_0 x \cos\left(\frac{h_c}{R} z\right), \end{aligned} \tag{1}$$

where $x' \equiv dx/ds$, z is the longitudinal displacement from the rf bucket center, $p = \beta E/c$ is the momentum, $C = 2\pi R$ is the circumference, and the strength K_0 of crabbing is related to the peak voltage V_{c0} of the cavity by

$$K_0 = \frac{qeV_{c0}h_c}{RE}, \tag{2}$$

with qe the electric charge of the particle, and h_c, an integer, the harmonic number of the cavity. If the crabbing wavelength is much larger than the bunch length, i.e.,

$$\frac{2\pi R}{h_c} \gg \sigma_z, \tag{3}$$

the kick in x' is approximately linearly proportional to the displacement z. At the IP, this kick results in a z-dependence of the horizontal displacement x. Thus, the bunch can be tilted by an angle $\alpha/2$ in the x–z plane with $\tan(\alpha/2) \approx \sqrt{\beta_0 \beta^*} K_0$, where β^* and β_0 are the β functions at the IP and the cavity (s_0), respectively. The voltage required is thus

$$qeV_{c0} = \frac{RE}{h_c \sqrt{\beta_0 \beta^*}} \tan\frac{\alpha}{2}. \tag{4}$$

Obviously, for given α and β^*, a high-β location and a high operational frequency (or harmonic number h_c) is preferred for the cavity, provided that the condition Eq. 3 is satisfied. The second cavity located at s_1 with a betatron phase of $+90°$ from the IP needs to operate at a voltage

$$V_{c1} = \sqrt{\frac{\beta_0}{\beta_1}} V_{c0} \tag{5}$$

to restore the particle motion to its unperturbed state.

For the high-field hadron collider, the crab cavities can be positioned at places with $\beta_0 \approx 50$ km. With a frequency of 379 MHz, the required voltage for the transverse cavities is between 3.2 and 4.4 MV for a crossing angle α between 70 and 97 μr, as shown in Table I.

B. Dispersive Crabbing

An alternative scheme for crab crossing is to employ two *regular* (instead of *transverse deflecting*) cavities located at dispersive regions, where the betatron phase advances are $\pm 180°$ from the IP. At the first cavity where the dispersion is η_0, the particle receives a kick $\Delta\delta$ in momentum,

$$\Delta\delta = \frac{qeV_0}{\beta^2 E} \sin\left(\frac{h_0}{R} z\right), \tag{6}$$

Table I: Comparison between nominal and crabbing operations.

Quantity	Unit	Nominal	Crab I	Crab II
β^*	m	0.1	0.1	0.05
α	μr	70	70	97
V_{rf}	MV	100	10	10
V_{crab}	MV	0	3.2	4.4
f_{crab}	MHz	–	379	379
σ_z	mm	22	41	41
$\mathcal{L}_{ini}$	10^{34} cm^{-2}s^{-1}	1.1	1.1	2.2

which results in an offset in the betatron closed orbit,

$$\Delta x_{\beta 0} = -\eta_0 \Delta\delta, \tag{7}$$

where V_0 and h_0 are the peak voltage and harmonic number of the rf cavity. At the IP where the dispersion is zero, the bunch is tilted by an angle $\alpha/2$, with

$$\tan\frac{\alpha}{2} \approx -\sqrt{\frac{\beta^*}{\beta_0}} \frac{\Delta x_{\beta 0}}{z}. \tag{8}$$

The voltage V_0 required is thus

$$qeV_0 = \frac{RE\beta^2}{h_0 \eta_0} \sqrt{\frac{\beta_0}{\beta^*}} \tan\frac{\alpha}{2}. \tag{9}$$

A second cavity located at a place with a betatron phase of $+180°$ from the IP operates at the same voltage as the first one to restore the particle motion. The dispersion and β function at the second cavity needs to be the same as at the first one.

The dispersive scheme usually requires a large dispersion at the cavity locations along with a large operating rf voltage. For the high-field collider, the rf cavities are assumed to be positioned at places with $\beta_0 \approx 200$ m. Even with a high dispersion of $\eta_0 = 10$ m, an impractically high voltage of more than 1 GV is required for a $\alpha = 70\mu$r crossing. Furthermore, since the required dispersions at the two cavities are the same, additional dipoles are needed to make the dispersion at the IP zero. The longitudinal slippage between the two cavities produced by these dipoles will inevitably degrade the crabbing accuracy.

C. η^* Crabbing

Another scheme for crab crossing is *not* to employ any dedicated cavities. Instead, the storage rf cavity is placed near the IP, and the dispersion η^* at the IP is made non-zero. With a peak voltage V_{rf} and harmonic number h, the rf cavity changes the momentum of the particle,

$$\Delta\delta = \frac{qeV_{rf}}{\beta^2 E} \sin\left(\frac{h}{R} z\right). \tag{10}$$

Due to the dispersion η^*, the horizontal displacement at the IP resulting from this momentum change produces a tilt in the bunch with $\tan(\alpha/2) \approx \eta^* \Delta\delta/z$. The voltage required is thus

$$qeV_{rf} = \frac{RE\beta^2}{h\eta^*} \tan\frac{\alpha}{2}. \tag{11}$$

For a moderate voltage V_{rf}, this scheme often requires a large dispersion η^* at the IP. Such a dispersion effectively enlarges the horizontal beam size σ^* at the IP, which inevitably causes a degradation in luminosity. Furthermore, the dispersion modulates the beam-beam interaction to give nonlinear synchro-betatron coupling.

For the high-field collider, we assume that an rf cavity of 50 MV is located near each one of the two IPs. To achieve an angle of $\alpha = 70\mu$r, the η^* needed is more than 4 m. With a momentum spread of $\sigma_p \approx 2 \times 10^{-5}$ in the beam, such a large dispersion makes the spot size at the IP intolerably large.

III. THEORETICAL ANALYSIS

In this Section, we develop a Hamiltonian formalism to study the dynamics of deflection crab crossing, which so far is the only practical scheme for the high-field hadron collider. Using this formalism, we evaluate the sensitivity of beam quality and machine performance to errors in voltage and phase matching of the crab cavities. A matrix formalism is also introduced for the linearized system to describe the coupling.

A. Hamiltonian Formalism

The single-particle motion can be described by a Hamiltonian expressed in terms of the variables $(x, p_x, y, p_y, \phi, W; s)$ as

$$H = H_0 + H_1, \tag{12}$$

where $\phi = -hz/R$ is the rf phase, $W \equiv -\Delta E/h\omega_s$, ω_s is the angular revolution frequency, and $\Delta E = \beta c \Delta p$. Here, H_0 governs the unperturbed particle motion,[11, 12]

$$\begin{aligned} H_0 &= -p + \frac{1}{2p}\left(p_x^2 + p_y^2\right) + \frac{p}{2}\left(K_x x^2 + K_y y^2\right) - \\ &\quad - \frac{h^2\omega_s^2}{2\beta^3 Ec}\left(\frac{\eta_x}{\rho} - \frac{1}{\gamma^2}\right) W^2 - \\ &\quad - \frac{qeV}{h\omega_s}\sum_{n=-\infty}^{\infty}\delta(s - nC)\cdot \\ &\quad \cdot\left\{\cos\left[\phi_s + \phi + \frac{hs}{R} - \frac{h}{Rp}\left(\eta_x p_x - p\eta_x' x\right)\right] + \right. \\ &\quad \left. + \sin\phi_s \cdot \left[\phi - \frac{h}{Rp}\left(\eta_x p_x - p\eta_x' x\right)\right]\right\}, \end{aligned} \tag{13}$$

with η_x the dispersion, $\eta_x' = d\eta_x/ds$, and H_1 represents the contribution from the two crab cavities of strength K_0 and K_1 located at s_0 and s_1, respectively,

$$\begin{aligned} H_1 &= \frac{pR}{h_c} x \sin\left(\frac{h_c}{h}\phi\right)\cdot \\ &\quad \cdot \sum_{n=-\infty}^{\infty}\left[K_0\delta(s - nC - s_0) + K_1\delta(s - nC - s_1)\right]. \end{aligned} \tag{14}$$

For simplicity without losing generality, we assume that the crab cavities operate at the same frequency as the storage rf system ($h_c = h$), and that the machine operates above transition in storage mode with the synchronous phase $\phi_s = \pi$. We average the contribution of the storage rf cavities over the circumference, and define

$$C_\phi \equiv \frac{qeV}{\pi h}, \quad \text{and} \quad C_W \equiv \frac{h^2\omega_s^2\eta}{2E\beta^2}, \tag{15}$$

where $\eta = \langle \eta_x/\rho \rangle - 1/\gamma^2$ is the slippage factor. The Hamiltonian (Eq. 13) can be expressed in terms of the action-angle variables $(\psi_x, J_x, \psi_y, J_y, \psi_z, J_z; s)$ using a canonical transformation. The new variables are related to the old ones as

$$\begin{aligned} x,\, y &= \sqrt{\frac{2\beta_{x,y}J_{x,y}}{p}}\cos(\nu_{x,y}\phi_{x,y} + \psi_{x,y}), \\ p_{x,y} &= -\sqrt{\frac{2pJ_{x,y}}{\beta_{x,y}}}\left[\alpha_{x,y}\cos(\nu_{x,y}\phi_{x,y} + \psi_{x,y}) + \right. \\ &\qquad \left. + \sin(\nu_{x,y}\phi_{x,y} + \psi_{x,y})\right], \\ \phi &= 8\sum_{m=1,odd}^{\infty}\frac{c_m}{m}\cos\left[m\left(-\nu_z\theta + \psi_z\right)\right], \\ W &= \frac{2\pi}{\mathrm{K}(k)}\sqrt{\frac{C_\phi}{C_W}}\sum_{m=1,odd}^{\infty} c_m \sin\left[m\left(-\nu_z\theta + \psi_z\right)\right], \end{aligned} \tag{16}$$

where the betatron phase $\phi_{x,y}$ and the azimuthal angle θ are defined as

$$\phi_{x,y} \equiv \int \frac{ds}{\nu_{x,y}\beta_{x,y}}, \quad \theta \equiv \frac{s}{R}. \tag{17}$$

The nonlinear synchrotron motion of ϕ and W is reflected by the series expansion with the coefficients

$$c_m \equiv \frac{\xi^{m-\frac{1}{2}}}{1 + \xi^{m-\frac{1}{2}}}, \quad \xi \equiv \exp\left[-\frac{\pi \mathrm{K}(\sqrt{1-k^2})}{\mathrm{K}(k)}\right], \tag{18}$$

$k = \sqrt{H_0/C_\phi} \leq 1$ is related to the action variable J_z by the relation

$$J_z = \oint W d\phi = 8\sqrt{\frac{C_\phi}{C_W}}\left[(k^2 - 1)\mathrm{K}(k) + \mathrm{E}(k)\right], \tag{19}$$

where $\mathrm{K}(k)$ and $\mathrm{E}(k)$ are the complete elliptical integrals[13] of first and second kind. The unperturbed synchrotron tune ν_z can be expressed in terms of the linear tune ν_{s0} as

$$\nu_z = \frac{\pi}{2\mathrm{K}(k)}\nu_{s0}, \quad \nu_{s0}\omega_s = \sqrt{C_\phi C_W}. \tag{20}$$

Using the relation[14, 15] $\sin\phi = \nu_{s0}^{-2} d^2\phi/d\theta^2$, the new Hamiltonian can be obtained as $\tilde{H}_0 = 0$, and

$$\begin{aligned} \tilde{H}_1 &= -\sum_{n=-\infty}^{\infty}\left[K_0\delta(s - nC - s_0) + K_1\delta(s - nC - s_1)\right]\cdot \\ &\quad \cdot \frac{2\pi^2 R}{h\mathrm{K}^2(k)}\left(2p\beta_x J_x\right)^{1/2}\cos(\nu_x\phi_x + \psi_x)\cdot \\ &\quad \cdot \sum_{m=1,odd}^{\infty} m c_m \cos\left[m\left(-\nu_z\theta + \psi_z\right)\right]. \end{aligned} \tag{21}$$

Note that the dependence on the longitudinal action J_z is contained in c_m and k.

B. Error-Induced Coupling Resonance

Eq. 21 indicates that if the crabbing is not completely compensated, synchro-betatron couplings can be excited. Suppose that $\Delta\phi$ is the deviation of the betatron phase advance from 180° between the two crab cavities, and that ΔK is the deviation of the crabbing strength from the matching value,

$$\phi_1 - \phi_0 = \pi + \Delta\phi, \quad \text{and} \quad K_1 = \sqrt{\frac{\beta_0}{\beta_1}}(K_0 + \Delta K). \tag{22}$$

Keeping only slowly varying resonance terms satisfying

$$\nu_x \pm m\nu_z = l + \epsilon, \quad \epsilon \ll 1, \quad m = \text{odd}, \tag{23}$$

and performing another canonical transformation with

$$\begin{aligned} \tilde{J}_x &= J_x, \qquad \tilde{\Psi}_x = \Psi_x, \\ \tilde{J}_z &= J_z, \qquad \tilde{\Psi}_z = \Psi_z \pm \frac{\epsilon}{m}\frac{s}{R}, \end{aligned} \tag{24}$$

the final Hamiltonian becomes

$$H_0 = \pm\frac{\epsilon}{mR}J_z, \tag{25}$$

$$\begin{aligned} H_1 \;=\; & -\sum_{n=-\infty}^{\infty}\left[K_0\delta(s - nC - s_0) + K_1\delta(s - nC - s_1)\right]\cdot \\ & \cdot\frac{m\pi^2 Rc_m}{h\mathrm{K}^2(k)}\left(2p\beta_x J_x\right)^{1/2}\cos\left(\psi_x \mp m\psi_z\right), \end{aligned} \tag{26}$$

where the tildes in J and Ψ are omitted for brevity. From Eq. 26 and the canonical equations of motion, the relation

$$mJ_x \pm J_z = \text{constant} \tag{27}$$

holds near a resonance $\nu_x \pm m\nu_z = l$. Hence, the growth in action is limited for a sum (or difference) resonance above (or below) transition. However, since J_x is usually much smaller than J_z, the growth in the betatron amplitude is important even for a difference resonance above transition.[12] The change of action J_x and J_z in one revolution can be evaluated as

$$\begin{aligned} \Delta J_x \;=\; & -\frac{m\pi^2 Rc_m}{h\mathrm{K}^2(k)}\left(2p\beta_x J_x\right)^{1/2}\left[K_0\sin\left(\psi_x \mp m\psi_z\right) + \right. \\ & \left. +(K_0 + \Delta K)\sin\left(\psi_x \mp m\psi_z + \Delta\phi\right)\right], \\ \Delta J_z \;=\; & \mp m\Delta J_x. \end{aligned} \tag{28}$$

Defined the rms horizontal emittance ϵ_x and longitudinal bunch area S,

$$\epsilon_x = \frac{2}{p}\langle J_x\rangle \quad \text{and} \quad S = 2\pi\langle J_z\rangle, \tag{29}$$

where $\langle\ \rangle$ denotes the average over all the particles. The growth rate of the emittance ϵ_x can be obtained as

$$\begin{aligned} \frac{1}{\epsilon_x}\frac{d\epsilon_x}{dt} \;=\; & \frac{2m\langle c_m\rangle\beta cK_0}{\pi h}\left(\frac{2\beta_0}{\epsilon_x}\right)^{1/2}\cdot \\ & \cdot\left[\left(\frac{\Delta K}{K}\right)^2 + (\Delta\phi)^2\right]^{1/2}. \end{aligned} \tag{30}$$

For a difference (or sum) resonance above (or below) transition, the growth rate of the bunch area S is

$$\begin{aligned} \frac{1}{S}\frac{dS}{dt} \;=\; & \frac{2m^2\langle c_m\rangle K_0\beta^2 E}{hS}\left(2\beta_0\epsilon_x\right)^{1/2}\cdot \\ & \cdot\left[\left(\frac{\Delta K}{K}\right)^2 + (\Delta\phi)^2\right]^{1/2}, \end{aligned} \tag{31}$$

where the quantity $\langle c_m\rangle$ can be approximated by[14]

$$\langle c_m\rangle \approx \left(\frac{\langle\phi_{max}\rangle}{8}\right)^m, \quad \langle\phi_{max}\rangle^2 \approx \frac{h^2\eta\omega_s S}{\pi\beta^2 E\nu_z}, \tag{32}$$

with ϕ_{max} the maximum phase of the particle synchrotron oscillation.

For a hadron storage ring, the synchrotron tune is usually small. The number m satisfying the resonance condition Eq. 23 is very large. In the case of the high-field collider, $\nu_z \approx 0.003$, $\phi_{max} = 0.18$, and $\langle c_m\rangle < 10^{-18}$ for $m > 10$. The emittance growth caused by the synchro-betatron coupling, which is excited by the crabbing errors, is negligible.

On the other hand, for an electron-electron or electron-positron storage ring collider, the synchrotron tune is often large. The mismatch in crabbing voltage and phase can excite strong synchro-betatron couplings of low order m, which results in emittance growth in both horizontal and longitudinal directions.

C. Off-Resonance Crabbing Degradation

Even though the beam is off resonance, the perturbation in action can still make the crabbing process less accurate. If $\Delta\nu_x$ is the average horizontal tune spread in the bunch, the characteristic decoherence time for the betatron motion is $\Delta\nu_x^{-1}$ turns. The off-resonance condition for an accurate crabbing is thus

$$\frac{1}{\Delta\nu_x}\frac{\Delta\epsilon_x}{\epsilon_x} \ll 1. \tag{33}$$

Using Eqs. 28, 29, and 32 with $m = 1$, this condition can be sufficiently met if the accuracy of voltage and betatron-phase matching between the two cavities satisfies

$$\left[\left(\frac{\Delta K}{K}\right)^2 + (\Delta\phi)^2\right]^{1/2} \ll \frac{2h\omega_s\Delta\nu_x}{\langle\phi_{max}\rangle\beta cK_0}\left(\frac{\epsilon_x}{2\beta_0}\right)^{1/2}, \tag{34}$$

where $\langle\phi_{max}\rangle$ is given by Eq. 32.

For the high-field hadron collider, the tune spread produced by beam-beam interactions, magnetic multipoles, etc. is of the order 10^{-3}. If the tolerable deviation in ϵ_x is 1%, the matching crabbing voltage needs to be accurate to about 1%, and the betatron phase advance between the two cavities needs to be within about 2° of 180° (Eq. 34).

D. Matrix Formalism

The coupling between the horizontal and longitudinal motion caused by imperfect crabbing can also be illustrated by a matrix formalism. Consider the one-turn matrix at the location of the deflection crabbing cavity, $-90°$ betatron phase from the IP, for

variables (x, x', z, δ). The matrix can be derived by linearizing the kicks by the crabbing cavities,

$$\begin{bmatrix} \mathbf{M} & \mathbf{n} \\ \mathbf{m} & \mathbf{N} \end{bmatrix} \tag{35}$$

where, to the first order of error in strength ΔK and phase $\Delta\phi$,

$$\begin{aligned}
\mathbf{M} &= \begin{bmatrix} \cos\mu_x + \alpha_0 \sin\mu_x & \beta_0 \sin\mu_x \\ -\alpha_0 \cos\mu_x \Delta\phi & \\ -\dfrac{1+\alpha_0^2}{\beta_0}\sin\mu_x & \cos\mu_x - \alpha_0 \sin\mu_x \end{bmatrix} \\
\mathbf{N} &= \begin{bmatrix} 1 - C\eta U + C\eta\beta_0 K_0^2 \Delta\phi & -C\eta \\ U - \beta_0 K_0^2 \Delta\phi & 1 \end{bmatrix} \\
\mathbf{m} &= \begin{bmatrix} C\eta(\alpha_0 K_0 \Delta\phi + \Delta K) & C\eta\beta_0 K_0 \Delta\phi \\ -\alpha_0 K_0 \Delta\phi - \Delta K & -\beta_0 K_0 \Delta\phi \end{bmatrix} \\
\mathbf{n} &= \begin{bmatrix} \beta_0(K_0 \cos\mu_x \Delta\phi - \sin\mu_x \Delta K) & 0 \\ -K_0(\sin\mu_x + \alpha_0 \cos\mu_x)\Delta\phi & 0 \end{bmatrix},
\end{aligned} \tag{36}$$

where $U = qeV_{rf}h/RE\beta^2$, $\mu_x = 2\pi\nu_x$, and α_0 and β_0 are the lattice functions at s_0. The amount of global x–z coupling is often characterized[7] by the quantity

$$\begin{aligned}
\det(\mathbf{m} + \mathbf{n}^\dagger) &= K_0^2 C\eta\beta_0 \left[-(\Delta\phi)^2 \sin\mu_x + \right. \\
&\quad + \Delta\phi \frac{\Delta K}{K_0}(\cos\mu_x - \alpha_0 \sin\mu_x) - \\
&\quad \left. - \left(\frac{\Delta K}{K_0}\right)^2 \sin\mu_x \right].
\end{aligned} \tag{37}$$

For the high-field collider with a matching error of 10^{-2}, $\det(\mathbf{m} + \mathbf{n}^\dagger)$ is of the order of 10^{-10}, i.e., the global x–z coupling is very small.

IV. CONCLUSIONS AND DISCUSSION

In this paper, we have reviewed the principle and operational requirements of various crab crossing schemes for storage ring colliders. A Hamiltonian formalism has been developed to study the crabbing dynamics. Using this formalism, we evaluate the sensitivity of crabbing performance to errors in voltage and phase matching of the crab cavities. The emittance growth caused by matching error induced synchro-betatron coupling is also estimated. Requirements are obtained for the voltage and frequency of the crab cavities to achieve a head-on collision during angle crossing, and for the accuracy of voltage and phase matching in a deflection crabbing scheme.

For the high-field hadron collider, a deflection crabbing scheme can be used to reduce β^* from 0.1 m to 0.05 m and below. At the same time, luminosity degradation caused by the angle crossing is eliminated, as shown in Table I. Since a longer bunch length can be tolerated when crab crossing is employed, the required voltage of the 379 MHz storage rf system is greatly reduced from 100 MV to about 10 MV. With the same frequency of 379 MHz operating in a transverse mode, the required voltage for the crab cavities is about 3.2 MV for $\beta^* = 0.1$ m, and 4.4 MV for $\beta^* = 0.05$ m. The needed relative accuracy of voltage and betatron-phase matching is about 1%. The beam emittance growth caused by error-induced synchro-betatron coupling is negligible.

V. ACKNOWLEDGMENTS

The author would like to thank G. Dugan, M. Harrison, and S. Peggs for many helpful discussions.

VI. REFERENCES

[1] *Energy Scaling, Crab Crossing and the Pair Problem*, R. B. Palmer, Invited talk at the DPF Summer Study Snowmass 88, SLAC-PUB-4707, Stanford 1988.

[2] *Beyond the LHC: A Conceptual Approach to a Future High Energy Hadron Collider*, M. J. Syphers, M. A. Harrison, S. Peggs, Dallas, PAC Proc., 1995, p. 431.

[3] *Really Large Hadron Colliders*, G. Dugan, Invited talk at 1996 DPF/DPB Summer Study on New Directions for High-Energy Physics, Snowmass, 1996.

[4] *Dispersive Crab Crossing: An Alternative Crossing Angle Scheme*, G. Jackson, Fermilab Note, FN-542, 1990.

[5] *Single Beam Crab Dynamics*, T. Chen and D. Rubin, Conf. Record of 1991 IEEE Oart. Accel. Conf., Vol. 3 LBL, SLAC, LANL, San Francisco (1991), p. 1642.

[6] *Beam-Beam Collision Scheme for Storage-Ring Colliders*, K. Oide, K. Yokoya, Physical Review A, **40**, 315 (1989).

[7] *Angle Crossing of Bunched Beams in Electron Storage Rings*, T. Chen, Ph. D. Dissertation, Cornell University, 1993.

[8] *International Linear Collider Technical Review Committee Report*, 1995.

[9] *CESR-B Conceptual Design for a B Factory Based on CESR*, CESR Group, CLNS 91-1050, 1991.

[10] *Interaction Region Analysis for a High-Field Hadron Collider*, J. Wei, et. al., these proceedings (1996).

[11] *An Introduction to the Physics of Particle Accelerators*, M. Conte and W. W. MacKay, World Scientific Pub. Co., Singapore, 1991.

[12] *Synchro-betatron Resonance Driven by Dispersion in RF Cavities*, T. Suzuki, Particle Accelerators, **18**, 115 (1985).

[13] *Beam Life-Time with Intra-beam Scattering and Stochastic Cooling*, J. Wei and A. G. Ruggiero, Proc. 1991 Particle Accelerator Conference, San Francisco, 1869-1871 (1991).

[14] *Synchro-betatron Resonance Driven by Dispersion in RF Cavities: A Revised Theory*, R. Baartman, TRIUMPH Design Note, TRI-DN-89-K40 (1989).

[15] *Hamiltonian Treatment of Synchro-betatron Resonances*, G. Guignard, *CERN Fifth Advanced Accelerator Physics Course*, ed. S. Turner, 1995, p. 187.

INTERACTION REGION ANALYSIS FOR A HIGH-FIELD HADRON COLLIDER

Jie Wei and Stephen G. Peggs
Brookhaven National Laboratory, Upton, NY 11973, USA
Glen P. Goderre
Fermi National Accelerator Laboratory, Batavia, IL 60510, USA

ABSTRACT

The primary goal of the interaction region (IR) is to de-magnify the transverse beam dimension to a small spot size at the interaction point (IP) to reach the required luminosity. With an experimental drift space of ± 25 m and a quadrupole focusing strength of 360 T/m at the triplets, a β^* of 0.1 m can be achieved at a beam energy of 50 TeV. Only two families of sextupoles are needed to globally correct the chromaticity. Since the momentum spread of the beam is small ($\sigma_p \approx 2 \times 10^{-5}$), a relatively large (about 20) linear chromaticity can be tolerated so that higher-order chromatic aberration produced by the low-β^* optics is negligible. With a crossing angle of 70 μr and a beam separation of 5 σ, the required minimum aperture of the triplet magnets is about 3 cm. The luminosity reduction resulted from such a crossing angle is about 13%.

Crab crossing can be used to further reduce β^* to below 0.05 m. At the same time, luminosity degradation caused by the angle crossing is eliminated. With crab cavities positioned near the triplet operating at a voltage of a few MV, the required voltage of the 379 MHz storage rf system can be reduced from the nominal 100 MV to below 10 MV. The requirements on the accuracy of the positioning of the crab cavities and the operating voltage are both moderate. More than two families of sextupoles are needed for global chromatic compensation only when β^* approaches 0.05 m and below.

I. INTRODUCTION

The design goal of a high-field hadron collider (RLHC)[1, 2, 3] is a 50 TeV storage ring that can achieve a peak luminosity of 10^{34} cm^{-2}·s^{-1} with a small number of interactions per bunch-bunch collision. Table I lists the major parameters of this machine in comparison with LHC and SSC. For a round hadron beam of rms transverse beam size σ^* at collision, the luminosity can be expressed as

$$\mathcal{L}_0 = \frac{N_B N_0^2 f}{4\pi\sigma^{*2}}, \qquad (1)$$

where N_B is the number of bunches in each ring, N_0 is the number of particles in the bunch, and f is the revolution frequency. Among the quantities that determine the luminosity[3] in Eq. 1, the beam emittance reaches an equilibrium value of 0.2πmm·mr after about 5 hours of storage due to significant synchrotron radiation (damping time $\tau_{damp} \approx 1.2$ h). The number of particles N_0 per bunch is limited by the constraints from the number of interactions per crossing, beam-beam tune shift, and instabilities. The total number of particles $N_B N_0$ is further limited by the cryogenic constraints on radiation power. Therefore, the lattice function β^* at the interaction point (IP) must be small to reach the design luminosity.

Table I: Comparison of major operational parameters between RLHC, LHC, and SSC at beam storage.

Quantity	Unit	SSC	LHC	RLHC
E_s	TeV	20	7	50
C	km	83	27	95
B_0	T	6.6	8.4	12.6
β^*	m	0.5	0.5	0.1
α	μr	75	200	70
$\epsilon_{N,rms}$	mm·mr	1.0	3.8	1.0
S	eV·s	0.73	0.63	0.22
f_{rf}	MHz	375	400	379
V_{rf}	MV	20	16	100
τ_{sep}	ns	16	25	32
τ_{damp}	hour	12.5	12.9	1.2
N_0	10^{10}	0.73	10.5	0.75
$N_B N_0$	10^{14}	1.27	2.98	0.75
$\mathcal{L}_{ini}$	10^{34} cm^{-2}s^{-1}	0.1	1.0	1.1

The primary goal of the interaction region is to de-magnify the transverse beam dimension to a small spot size at the IP to reach the required luminosity. In Section II, we discuss various constraints that determine the practically achievable β^*. Field quality requirements on magnet construction and alignment are discussed in Section III. The effects of synchrotron radiation are estimated in Sections IV. Conclusions and a discussion are given in Section V.

II. CONSTRAINTS ON IR DESIGN

The approach towards achieving an infinitesimal β^* is limited by various conditions. In this section, we first discuss the conditions on the crossing angle and beam separation, and then summarize the limitations imposed by the angle-crossing luminosity degradation, hourglass effect, chromatic aberrations, and triplet aperture and gradient constraints. Finally, IR parameters for the high-field collider are presented.

A. Crossing Angle and Beam Separation

To enjoy the benefits of a relatively small bunch spacing, the beams must cross at an angle α to avoid more than one bunch-bunch collision in each experimental straight section, i.e.,

$$\frac{\alpha\beta^*}{\sigma^*} = n_\alpha \gg 1, \qquad (2)$$

where n_α is usually chosen to be larger than 5. A non-zero crossing angle causes a degradation in luminosity,

$$\mathcal{L} = \mathcal{L}_0 R_\alpha, \quad R_\alpha = \left(1 + \frac{\alpha^2 \sigma_z^2}{4\sigma^{*2}}\right)^{-1/2}, \tag{3}$$

where $\mathcal{L}_0$ is given by Eq. 1, and σ_z is the rms longitudinal bunch length. α must also be chosen so that the condition

$$\frac{\alpha \sigma_z}{\sigma^*} \ll 1 \tag{4}$$

is satisfied.

The luminosity degradation can be eliminated by using a pair of crab[5] cavities (rf cavities operating on their transverse modes) near the IP to make the angle-crossing beams collide head-on. A brief discussion of crab crossing will be given in Section VI. Detailed studies on possible crab crossing scenarios are presented in Ref. [6].

B. Hourglass Effect

In the experimental space near the IP, the transverse β function varies according to the relation

$$\beta(s) = \beta^* + \frac{s^2}{\beta^*}, \tag{5}$$

where s is the distance from the IP. When β^* is comparable to the longitudinal bunch dimension σ_z, this variation results in a reduction of luminosity (so called Hourglass effect)

$$\mathcal{L} = \mathcal{L}_0 R_H, \quad R_H = \frac{2}{\sqrt{\pi}\sigma_z} \int_0^\infty \frac{\exp(-z^2/\sigma_z^2)}{1 + z^2/\beta^{*2}} dz. \tag{6}$$

The factor $R_H \approx 0.76$ if $\sigma_z = \beta^*$, and rapidly approaches unity when β^* is increased above σ_z.[4, 7] Unless novel approaches are adopted to make the focal point z-dependent (e.g., by introducing a coherent momentum spread in the bunch together with a partially uncompensated chromaticity), the condition

$$\beta^* > \sigma_z \tag{7}$$

has to be satisfied to avoid a significant luminosity degradation. The situation is unchanged with crab crossing, since crab cavities with limited voltage usually only tilt the bunch by a small amount.

C. Chromatic Aberrations

The strong focusing produced by the IR triplet quadrupoles needed to achieve a low β^* inevitably generates chromatic aberrations which requires correction with sextupole families. Expressing the momentum ($\delta \equiv \Delta p/p$) dependence of the transverse tunes ν as

$$\nu = \nu_0 + \xi_0 \delta + \xi_1 \delta^2 + O(\delta^3), \tag{8}$$

the linear and second-order chromaticity produced by a low-β^* insertion can be estimated[8, 9] as

$$\xi_0 \approx -\frac{1}{2\pi}\sqrt{\frac{\hat{\beta}}{\beta^*}}, \quad \text{and} \quad \xi_1 \approx -\frac{\hat{\beta}}{\beta^*}\cot\mu, \tag{9}$$

where the peak $\hat{\beta}$ at the triplet is inversely proportional to β^* for a given machine, and μ is the phase advance of the arc cell. When β^* is reduced, higher-order chromatic effects become increasingly important.

Above the transition energy, the goal of chromatic correction is to achieve a small and positive chromaticity for the entire beam, so that the machine can operate free from strong resonances and the head-tail instability. Since the dispersion is designed to be zero at the IP, and since the phase advance across the IP is π, the dispersion has opposite signs at the two triplets around the IP. Sextupoles for a local correction would have opposite strengths, and their non-linear kicks would act in phase, necessitating a compensation with additional sextupoles. Therefore, a global correction with multi-families of sextupoles is sometimes preferred.[9]

D. Triplet Location and Aperture

The low-β^* insertion quadrupoles are usually located at a certain distance from the IP for the placement of experimental detectors and solenoids. As β^* is reduced, the maximum β at the triplet increases proportionally according to Eq. 5. The aperture of the triplet quadrupoles must be large enough to provide adequate magnetic field quality. Let L^* be the free drift space between the IP and the triplet (Fig. 1), G and $K = G/B_0\rho$ be

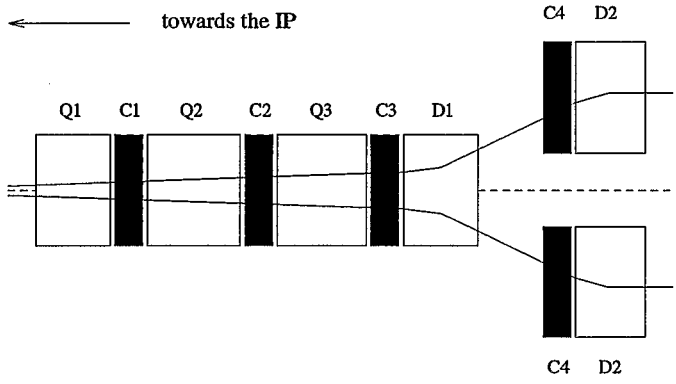

Figure 1: Schematic layout of the insertion-region magnets showing the dipoles (D1 and D2), quadrupoles (Q1, Q2, and Q3), and lumped corrector packages (C1, C2, C3, and C4) for the two counter-circulating beams.

the gradient and strength of the quadrupoles, with B_0 and ρ the dipole field and machine bending radius, respectively, Then, $\hat{\beta}$ can be approximately estimated as

$$\hat{\beta} \equiv \hat{L}^2 \beta^{*-1}. \tag{10}$$

The dependence of the effective distance $\hat{L}$ between the triplet and the IP on the quadrupole strength K and the free drift space L^* is shown in Fig. 2.[10] Typically, the dynamic aperture of the machine is close to the "good field aperture" defined as 2/3 of the magnet coil inner diameter (ID). Supposing that common triplet quadrupoles are used to contain both beams, their minimum coil ID (D_{trip}) can be obtained as

$$D_{trip} \approx 3\,\hat{L}\left(n_{GF}\frac{\sigma^*}{\beta^*} + \frac{\alpha}{2}\right), \tag{11}$$

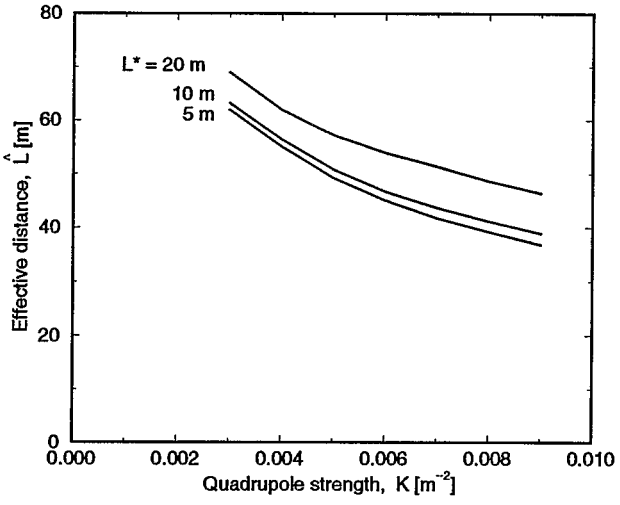

Figure 2: Effective distance $\hat{L}$ between the IR triplets and the IP as functions of quadrupole strength K and free drift space L^*.

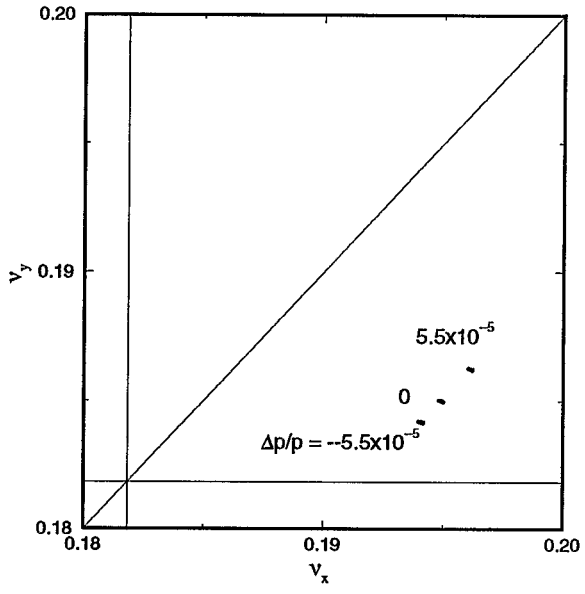

Figure 3: The tune footprint of an ideal lattice operating at $\beta^* = 0.1$ m. Resonance lines of order 15 and below are shown.

where the good field region contains $n_{GF}\sigma$ of the beam, and n_{GF} is typically chosen to be 7. With such a choice, a good beam lifetime is expected for the hadron beams.

E. Application to the High-Field Hadron Collider

For the currently proposed high-field hadron collider, two counter-circulating proton beams are stored in their separated rings of circumference 95 km at the energy of 50 TeV. With an experimental drift space of $2L^* = 50$ m and a focusing strength of 360 T/m at the triplet, the design β^* is equal to 0.1 m. From Fig. 2,[10, 11] we have $\hat{L} \approx 80$ m, and $\hat{\beta} \approx 64$ km. Assuming a 5σ separation ($n_\alpha = 5$) between the beams of an initial normalized rms emittance 1π mm·mr, the initial crossing angle α is 70 μr. This angle decreases from 70 μr to about 30 μr as the emittance is damped by synchrotron radiation. A minimum triplet coil ID of 32 mm provides good field region for 7σ beams.

With the rf system operating at a peak voltage (V_{rf}) 100 MV at frequency (f_{rf}) 379 MHz, the rms length (σ_z) of a bunch of longitudinal area (S) 0.22 eV·s at storage is about 2 cm. The rms relative momentum deviation σ_p is about 2×10^{-5}. From Eq. 6, the hourglass effect is negligible. The luminosity degradation caused by the crossing angle is about 13% (Eq. 1).

As β^* reaches 0.1 m, higher-order chromatic aberration produced by the low-β^* optics becomes noticeable. Fortunately, since the momentum spread of the beam is small, a relatively large ($\xi_0 = 20$) linear chromaticity can be tolerated so that higher-order aberration is negligible in comparison. With such a choice of linear chromaticity, only two families of sextupoles are needed for a global correction. Fig. 3 shows the 7σ tune footprints at the momentum deviation of $\Delta p/p = -2.5\sigma_p$, 0, and $2.5\sigma_p$, respectively, for the ideal lattice operating at $\beta^* = 0.1$ m. Both horizontal and vertical linear chromaticities after sextupole compensation are 20. Since the total (head-on plus long-range) beam-beam tune shift is about 0.008, the working point is free from all resonances of order below 10.

III. MAGNET FIELD ERROR COMPENSATION

The ultimate machine performance depends on achieving the highest possible magnetic field quality and alignment accuracy in the insertion-region triplet quadrupoles during low-β^* operation. In this section, we first explore the sources of error during magnet construction and alignments, and then present the compensation methods.

For the following discussions, the magnet body field is expressed in terms of the multipole series b_n and a_n defined at a reference radius R_0 by the relation

$$B_y + iB_x = 10^{-4}B_{ref}\left[\sum_{n\geq 0}(b_n + ia_n)\left(\frac{x+iy}{R_0}\right)^n\right], \quad (12)$$

where $B_{ref} = B_0$ for an arc dipole, and $B_{ref} = GR_0$ for a quadrupole. The transverse components of the fringe field can be defined similarly in terms of the integrated value.

A. Figure of Merit

Although the betatron phase advance is negligibly small across the triplet, the variation in transverse beam size is large from magnet body to end, and across the triplet. Therefore, error compensation of an undesired multipole b_n or a_n is based on minimizing the total action kick ΔJ in both horizontal and vertical directions across each triplet taking into account the variation of the design β-function[14] for both beams,

$$\frac{\Delta J_{x,y}}{J_{x,y}} \sim \frac{(2J)^{\frac{n-1}{2}}}{4\pi B_0\rho}\frac{10^{-4}B_{ref}}{R_0^n}\int_{triplet} b_n\beta_{x,y}^{\frac{n+1}{2}}\,ds \quad (13)$$

and

$$\frac{\Delta J_{x,y}}{J_{x,y}} \sim \frac{(2J)^{\frac{n-1}{2}}}{4\pi B_0\rho}\frac{10^{-4}B_{ref}}{R_0^n}\int_{triplet} a_n\beta_{x,y}^{\frac{n+1}{2}}\,ds, \quad (14)$$

where the integral to be minimized extends over all the quadrupole body and ends in one triplet. Typically, a multipole error is considered tolerable if $\Delta J_{x,y}/J_{x,y}$ summed over the ring satisfies

$$\frac{\Delta J_{x,y}}{J_{x,y}} \leq 5 \times 10^{-3}. \quad (15)$$

B. Error Sources

The leading sources of undesired harmonics are the design and construction errors in the placement of the coils at the ends and in the body of the magnets, e.g. large systematic b_5 and a_5 in the quadrupole lead ends, systematic b_5 and random b_2 in the quadrupole body.[13] The effect of the transverse fringe field contributed from the magnet ends is often significant. (On the other hand, the effect of the longitudinal fringe fields has been shown to be negligible.[12]) The secondary source is the mislocation of the iron yoke, which results in excitation dependent allowed multipoles b_5 and b_9 in the quadrupole body. According to Eq. 15, the tolerable systematic b_5 or a_5 for the 50 TeV high-field collider is about 0.5 unit at $R_0 = 10$ mm in the absence of correction.

The separation between the closed orbits of the two beams due to the non-zero crossing angle α produces a feed-down for the multipoles. The effective $\tilde{b}_{n-1}$ produced by a multipole b_n is approximately

$$\tilde{b}_{n-1} \approx \frac{n\alpha\hat{L}}{2R_0} b_n, \quad (16)$$

where $\hat{L}$ is defined by Eq. 10. For example, a b_5 of 0.5 units for the high-field collider will produce an effective $\tilde{b}_4$ of about 0.6 units.

The alignment procedure for the triplet assembly consists of many complicated steps. The accumulative errors from each step together with the complication caused by warm-cold transitions make it a challenging task to achieve an accurate alignment. Center offset of the quadrupoles will cause closed orbit distortion, while roll will cause transverse coupling.

C. Compensation Methods

Multipole optimization: Systematic multipole errors allowed by the geometrical symmetry (e.g., b_5 and b_9) should be minimized by iterating the coil cross section. The yoke should be designed so that its saturation helps to optimize the allowed multipoles at storage. Because of the large variation of beam transverse dimension and closed-orbit displacement from the magnet center axis, an error compensation between the fringe field and the body field of the magnet, which requires a simultaneous minimization of multipole action kick (Eq. 14) and feed-down (Eq. 16) for both beams, is difficult to achieve. A careful design is needed to eliminate errors at the magnet ends.

Shimming: Random errors in the magnet can be individually minimized by inserting tuning shims into the body after the magnet cold mass is constructed and measured. In the superconducting IR quadrupoles of the Relativistic Heavy Ion Collider, tuning shims are inserted into the 8 empty slots of the quadrupole body, whose variable thickness enables the individual minimization of 8 harmonics from a_2 to a_5 and from b_2 to b_5. Recent experiments at the Brookhaven National Laboratory indicates that random errors can be reduced to about 10% of their uncorrected values.[13] Similar measures should be adopted for the construction of the superconducting IR magnets of the high-field collider.

Choreographed welding: During assembly of the triplet packages, the welding can be choreographed to balance distortions and to minimize offsets. The magnetic center of the quadrupoles should be accurately located relative to the external fiducials, using techniques incorporating, for example, colloidal cells or magnetic antennas, after the magnets are fully assembled in the triplet package.

Local correctors: Lumped correctors located in the high-β IR region are highly effective in closed-orbit correction, local decoupling, and higher-order multipole error compensation. Fig. 1 schematically shows a possible corrector layout. Near the triplet, each beam sees a set of four corrector packages, each of 1 m length containing four corrector layers, as shown in Table II. Since the betatron phase advance is small across this high-β region, correction is localized. At a maximum strength of 10% of the arc dipoles (1.3 T), the two a_0 correctors are capable of correcting vertical closed-orbit deviations produced by an rms quadrupole center offset of about 0.2 mm. The b_0 corrector along with the independently adjustable dipole D2 are adequate to horizontally steer the beam into collision. The two a_1 correctors at a strength of 10% of the IR quadrupoles (36 T/m) can be used for local decoupling to compensate an rms quadrupole roll of about 1 mr. Since the β-function varies rapidly, higher-order multipole corrections (e.g., b_2 and b_5) in both horizontal and vertical directions can be best achieved with a total of four correctors for the two beams located at places with significantly different β_x/β_y ratio. The excitation strength of these higher-order correctors can be "dead-reckoned" based upon cold multipole measurements.

Table II: Contents of IR lumped corrector packages.

Layer	C1	C2	C3	C4
1	a_0/b_0	a_1	b_0/a_0	a_0
2	b_2	a_2	b_2	a_1
3	b_3	a_3	b_4	b_2
4	b_5	a_5	b_5	b_5

In addition to magnetic field errors, mechanical vibration of the triplets, often at a frequency of a few Hz, can easily cause the colliding beams to miss altogether. Feedback systems based on Beam Position Monitor measurements are necessary for a precise closed orbit control.

IV. SYNCHROTRON RADIATION POWER

With a damping time of about two hours, synchrotron radiation plays an important role in preserving the emittance during the collider performance. The cryogenic system must be designed to absorb the radiation energy generated by the circulating particles.

In the IR triplet region, the crossing angle causes an offset of the beam closed orbit from the quadrupole center axis. The

amount of radiation energy per unit length generated by a particle is

$$U = \frac{2r_0 m_0 c^2 \gamma^4}{3\rho^2}, \quad (17)$$

where r_0 is the classical radius of he particle, m_0c^2 is the rest energy, and γ is the relativistic factor. Compared with that in the regular arc dipole, the energy generated in the IR quadrupole can be estimated as

$$\frac{U(\text{triplet})}{U(\text{arc dipole})} \leq \left[\frac{(\alpha + 2n_{GF}\sigma^*\beta^{*-1})\hat{L}G}{2B_0}\right]^2 \approx 0.11, \quad (18)$$

where $G = 360$ T/m is the IR quadrupole gradient, and $B_0 = 12.6$ T is the arc dipole field strength. The cryogenic system must be designed to absorb this power at the triplet, and measures must be taken to prevent excessive radiation background at the IP.

V. CONCLUSIONS AND DISCUSSION

The approach towards achieving an infinitesimal β^* is mainly limited by the ability to correct chromatic aberration produced by the insertion region quadrupoles, and the ability to provide a short bunch length so that luminosity degradation is small (Eqs. 2, 4, and 7). With an experimental drift space of ± 25 m and a focusing strength of 360 T/m at the triplet quadrupoles, a β^* of 0.1 m can be achieved at the energy of 50 TeV. With the rf system operating at a peak voltage 100 MV at frequency 379 MHz, the bunch length σ_z is about 2 cm. The hourglass effect is therefore negligible. The crossing angle for a 5σ beam separation is 70μr. With such an angle, the luminosity reduction is about 13%. A minimum triplet coil ID of about 32 mm will provide a good field region for up to 7σ beams. Only two families of sextupoles are needed to globally correct the chromaticity.

Crab crossing can be used to further reduce β^* to 0.05 m and below. At the same time, luminosity degradation caused by the angle crossing is eliminated. Table III compares the nominal scheme, the crabbing scheme with $\beta^* = 0.1$ m, and with $\beta^* = 0.05$ m. With crab cavities positioned near the triplet operating at a voltage of 3.2~4.4 MV, the required voltage of the storage rf system can be reduced from the nominal 100 MV to about 10 MV, which still provides adequate bucket area A_B for the bunch. The requirements on the accuracy of the operating voltage and the positioning of the crab cavities are both moderate. Sextupoles of multiple families can be used to globally compensate the chromatic aberration.

Table III: Comparison between nominal and crabbing operations with $\beta^* = 0.1$ m and $\beta^* = 0.05$ m.

Quantity	Unit	Nominal	Crab I	Crab II
β^*	m	0.1	0.1	0.05
α	μr	70	70	97
D_{trip}	mm	32	32	45
V_{rf}	MV	100	10	10
A_B	eV·s	34	11	11
V_{crab}	MV	0	3.2	4.4
f_{crab}	MHz	–	379	379
σ_z	mm	22	41	41
σ_p	10^{-5}	1.9	1.0	1.0
R_α		0.87	1	1
σ^*	μm	1.4	1.0	1.0
$\mathcal{L}_{ini}$	10^{34} cm^{-2}s^{-1}	1.1	1.1	2.2

To achieve an even lower β^*, the bunch length needs to be reduced accordingly to avoid the hourglass effect. For example with $\beta^* = 0.025$ m, with crab crossing and a higher rf frequency of 758 MHz, the required rf voltage is about 100 MV. The ultimate challenge, however, is to achieve satisfactory chromatic compensation.

VI. ACKNOWLEDGMENTS

The authors would like to thank G. Dugan, M. Harrison, M. Syphers, and S. Tepikian for many helpful discussions.

VII. REFERENCES

[1] *Proceedings of the Workshop on Future Hadron Facilities in the US*, Bloomington, FERMILAB-TM-1907, 1994.

[2] *Beyond the LHC: A Conceptual Approach to a Future High Energy Hadron Collider*, M. J. Syphers, M. A. Harrison, S. Peggs, Dallas, PAC Proc., 1995, p. 431.

[3] *Really Large Hadron Colliders*, G. Dugan, Invited talk at 1996 DPF/DPB Summer Study on New Directions for High-Energy Physics, Snowmass, 1996.

[4] *Beam-Beam Instability*, A. Chao, AIP Conf. Proc. 127, *Physics of High Energy Particle Accelerators*, ed. M. Month, P.F. Dahl, M. Dienes, 1983, p. 202.

[5] *Energy Scaling, Crab Crossing and the Pair Problem*, R. B. Palmer, Invited talk at the DPF Summer Study Snowmass 88, SLAC-PUB-4707, Stanford 1988.

[6] *Crab Crossing in a Large Hadron Collider*, J. Wei, these proceedings, 1996.

[7] *Review of Linear Collider Beam-Beam Interaction*, P. Chen, AIP Conf. Proc. 184, *Physics of High Energy Particle Accelerators*, ed. M. Month, M. Dienes, 1989, p. 634.

[8] *Elementary Design and Scaling Considerations of Storage Ring Colliders*, A. Chao, AIP Conf. Proc. 153, *Physics of High Energy Particle Accelerators*, ed. M. Month, M. Dienes, 1987, p. 104.

[9] *Chromaticity*, A. Verdier, *CERN Fourth Advanced Accelerator Physics Course*, ed. S. Turner, 1992, p. 204.

[10] *Minimising Chromaticity in Interaction Regions with Long Weak Quadrupoles*, S. Peck, Proc. SSC Summer Study, Snowmass, 1984, p. 384.

[11] *Lattices for a High-Field 30 TeV Hadron Collider*, S. Peggs, et. al., these proceedings, (1996).

[12] *Theorem on Magnet Fringe Field*, J. Wei, R. Talman, Particle Accelerators, **55**, 339 (1996).

[13] *Large Aperture Quadrupoles for RHIC Interaction Region*, R. Gupta, et. al., Proc. 1993 Part. Accel. Conf., Washington, D.C., 1993, p. 2745.

[14] *Error Compensation in Insertion-Region Magnets*, J. Wei, Particle Accelerators, **55**, 439 (1996).

LATTICES FOR A HIGH-FIELD 30 TeV HADRON COLLIDER

S. Peggs, F. Dell, M. Harrison, M. Syphers, S. Tepikian, Brookhaven National Laboratory

ABSTRACT

Long arc cells would lead to major cost savings in a high field high T_c hadron collider, operating in the regime of significant synchrotron radiation. Two such lattices, with half cell lengths of 110 and 260 m, are compared. Both allow flexible tuning, and have large dynamic apertures when dominated by chromatic sextupoles. Lattices with longer cells are much more sensitive to systematic magnet errors, which are expected to dominate.

I. INTRODUCTION

Contemporary hadron colliders operate in a regime of insignificant synchrotron radiation damping. Conceptual designs of a high field post-LHC "Really Large Hadron Collider" (RLHC), with parameters only slightly beyond those of the SSC, benefit greatly from damping times much less than the storage time. They deliberately incorporate 'short' damping times to desensitize machine operations with respect to sources of phase space dilution, and to increase the integrated luminosity[1, 2]. High field RLHC designs explicitly use "high T_c" superconducting magnets, to safely absorb the radiation heat load of up to 5 W/m. They implicitly assume that the high T_c commercial magnets which are beginning to appear will, in due course, be developed into accelerator quality magnets. Magnet R&D based on recent advances in high T_c materials suggest the possibility of practical tape wound magnets[3].

This paper addresses lattice optimization issues, taking for granted the primary parameters listed in Table I that are discussed elsewhere[1, 2]. The advantages of very long arc cells are examined by studying two detailed lattices, one near each end of the spectrum of plausible arc cell length. The short cell lattice has 6 dipoles per half cell of length $L = 110$ m, while the long cell lattice has 15 dipoles per half cell of length $L = 260$ m. The optical and dynamical aperture performance of each lattice is discussed.

II. HALF CELL LENGTH

The optimum half arc cell length, L, depends on a dynamic balance between two effects pushing for longer cells, and one pushing for shorter cells. Longer cells save money through fewer quadrupoles, fewer correctors, and fewer spool pieces. They also have reduced strength chromaticity sextupoles, and an increased dynamic aperture from this source. However, shorter cells and smaller beams make more modest demands on magnetic field quality.

The SSC half cell length stayed remarkably constant at $L \approx 100$ m during repeated optimization exercises[4]. This is largely due to the consistent use of an almost invariant set of magnet error statistics, which assumed that random errors would dominate systematics. Recent experience with RHIC magnets shows (scaled) errors that are much smaller than in the SSC model, and shows, to the contrary, that systematics dominate randoms[5]. Measured errors in several real SSC dipoles were significantly smaller than in the standard SSC model used for tracking[6]. This suggests that RLHC half cells might be much longer than 100 meters.

Table I: Primary design parameters. Values which vary significantly with time, such as ϵ, are quoted at injection.

Parameter	units	value
Storage energy	[TeV]	30.0
Injection energy	[TeV]	1.0
Dipole field (store)	[T]	12.5
Dipole length	[m]	17.0
Dipole coil ID	[mm]	50 - 60
Triplet quad gradient (store)	[T/m]	300
Number of Interaction Regions		2
Transverse rms emittance, ϵ	[μm]	1.0
Longitudinal rms bunch area, S	[eV-s]	0.1
Longitudinal rms emittance, ϵ_s	[m]	.0102
RF frequency, f_{RF}	[MHz]	360
Transverse damping time (store)	[hr]	≈ 2.1

It is not yet possible to postulate a plausible magnet error model for high T_c dipoles. Instead, suppose that particle motion is stable within a "good field aperture" of $r_{GF} = 15$ mm, about half of the coil radius, in the arcs. If the phase advance per cell is 90 degrees, the maximum beta function is given by $\widehat{\beta} = 3.41\ L$, generating a maximum transverse rms injection beam size of

$$\widehat{\sigma}_\beta = \sqrt{\epsilon\widehat{\beta}/(\beta\gamma)} \tag{1}$$

The maximum allowable value of L occurs when the beam size fills the good field aperture. This is written as $r_{GF} = n\widehat{\sigma}_\beta$, where a conservative value for n is 15. This yields a maximum allowable half cell length of

$$\widehat{L} = \frac{\beta\gamma}{\epsilon}\frac{r_{GF}^2}{3.41\,n^2} = 313\ \text{[m]} \tag{2}$$

Long arc cells have a significant impact on longitudinal parameters, as shown in the values in Table II. The maximum dispersion, $\widehat{\eta} = 2.71\,L^2/R$, increases quadratically with L, causing the horizontal beam width contribution from momentum spread to rise much faster than the betatron contribution. The small momentum spreads quoted in Table II are determined

Table II: Longitudinal parameters for SHORT and LONG cell lattices, at injection. There are two sextupoles per cell.

Parameter	units	SHORT	LONG
Half cell length, L	[m]	110	260
Max. cell beta, $\widehat{\beta}$	[m]	376	898
Max. cell dispersion, $\widehat{\eta}$	[m]	3.85	22.9
Max. betatron size, $\widehat{\sigma}_\beta$	[mm]	.594	.918
Circumference, C	[km]	55.44	54.08
Horizontal tune, Q_x		65.195	28.195
Vertical tune, Q_y		66.185	29.185
Number of dipoles		2888	2900
Number of sextupoles		456	168
Slip factor, α	$[10^{-3}]$	.299	1.813
Mmtm. width, σ_p/p	$[10^{-3}]$	.1545	.0401
RMS bunch length, σ_s	[m]	.0619	.238
Synchrotron tune, Q_s	$[10^{-3}]$	6.59	2.63
Voltage slope, dV/ds	[MV/m]	103.29	2.78
RF voltage, V	[MV]	13.69	.37

by setting

$$\sigma_p/p = \widehat{\sigma}_\beta/\widehat{\eta} \tag{3}$$

to equalize the two contributions to the total beam width. The large slip factor in the LONG lattice ($\approx 1/Q_{arc}^2$) compensates for the small momentum width to make the beam acceptably resistant to collective effects, such as the microwave instability. The small LONG RF voltage (at 360 MHz) yields acceleration times of order 10^4 seconds.

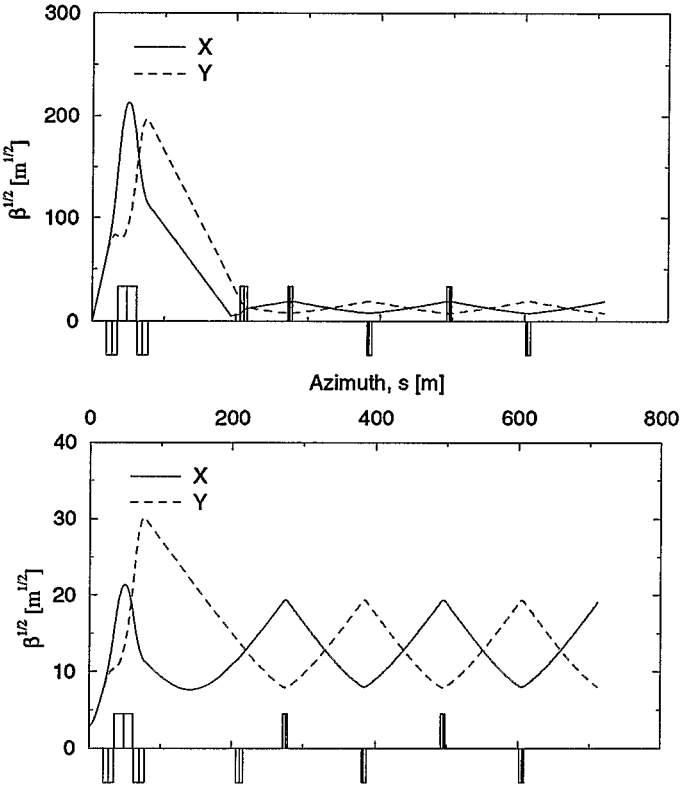

Figure 1: Telescope optics, with $\beta^* = 0.1$ m (storage) in the top figure, and $\beta^* = 8.0$ m (injection) in the bottom.

III. LATTICE OPTICS

Figure 1 shows a simple 4 quad telescope matching into empty arc cells. The telescope consists of a close packed triplet starting at $L^* = 20$ m from the collision point, followed by a 4th quadrupole placed $L/2$ from the first regular strength arc cell quadrupole [7]. The same optics also match into dispersion suppressor (DS) cells, as shown for the Interaction Regions (IR) cluster in Figure 2. Each DS has four 90 degree cells, with 3/4 the length of regular arc cells, and 2/3 of the number of dipoles. The 2 IRs are separated by back-to-back DSs, in addition to the DSs that match into the regular arcs. On the opposite side of the RLHC circumference are two utility straights of identical geometry, constructed from empty arc cells.

The maximum triplet gradient of 300 T/m causes peak and collision point betas to be related by an "effective length" L_e, defined by

$$\widehat{\beta} = L_e^2/\beta^* \tag{4}$$

and given by $L_e \approx 70$ m for both lattices [1, 8]. When $\beta^* = 0.1$ m at 30 TeV, the triplet beam size is $\sigma_{trip} \approx 1.2$ mm. Triplet quads can have modest bores.

IV. DYNAMIC APERTURE

When β^* is varied with the net chromaticities held constant ($\chi_x = \chi_y = 2.0$), the total sextupole strength has a contribution proportional to $1/\beta^*$, due to the natural chromaticity from the telescopes. Figure 3 illustrates this, with LONG strengths much weaker than the SHORT.

The ON momentum dynamic aperture is inversely proportional to the sextupole strength, as shown by the computed dynamic apertures recorded in Figure 4. Particles are launched with equal betatron motion amplitudes, parameterized by n where, if the motion is linear, $x_{max}/\sigma_x = y_{max}/\sigma_y = \sqrt{0.5}\,n$. The OFF momentum dynamic aperture is also plotted, for particles with a synchrotron oscillation amplitude of σ_p/p (injection value). In most cases the OFF and ON momentum dynamic apertures are indistinguishable, owing to the small momentum spread. The exception is the SHORT lattice with $\beta^* = 0.1$ m ($S_F = 24.4 \times 10^{-3}$ m^{-2}), where chromatic distortions due to the telescopes are at their strongest.

The huge dynamic apertures with only chromatic sextupoles present ($n_{DA} \geq 33$) are rather illusory, since neither a realistic physical aperture ($n \sim 40$) nor realistic dipole errors have been included. The apparent advantages of very long cells may disappear when realistic errors for tape wound high T_c magnets become known. Another paper in these Snowmass 96 proceedings makes a simple calculation of the tolerable systematic errors in arc dipoles, as a function of half cell length [9].

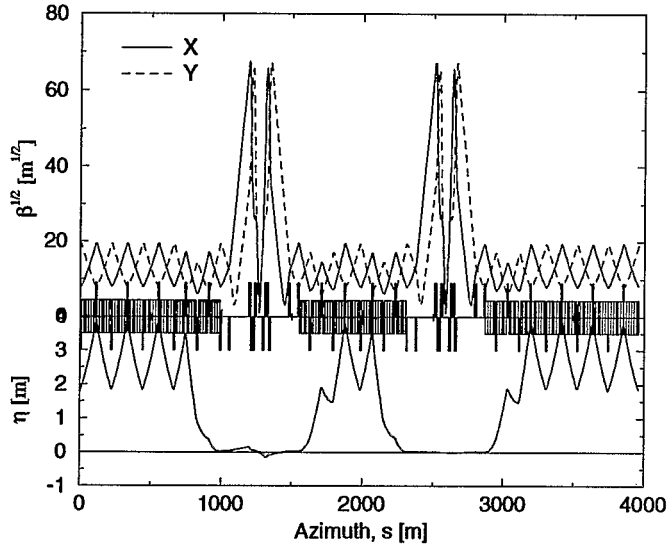

Figure 2: Layout of the IR cluster, with $\beta^* = 1.0$ [m].

V. CONCLUSIONS

Lattices with unusually long arc cells have potential advantages, including large cost savings, in a high field high T_c RLHC. Both LONG and SHORT lattices, with half cell lengths of 110 and 260 m, allow β^* to be squeezed down from 8.0 m at injection to 0.1 m at storage. However, to optimize the cell length it is necessary derive realistic magnet errors. This includes addressing the relative importance of random and systematic harmonics - do systematics dominate, as at RHIC, or do randoms dominate, as assumed for the SSC? [9] It is also necessary to explore the scaling of collective instabilities with respect to arc cell length.

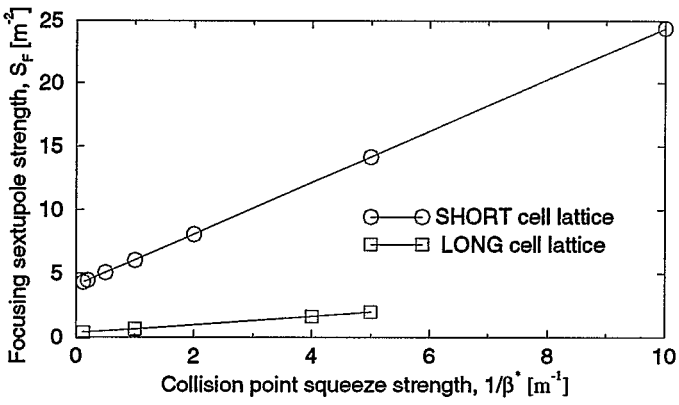

Figure 3: Chromaticity sextupole strength versus squeeze strength at constant net chromaticity.

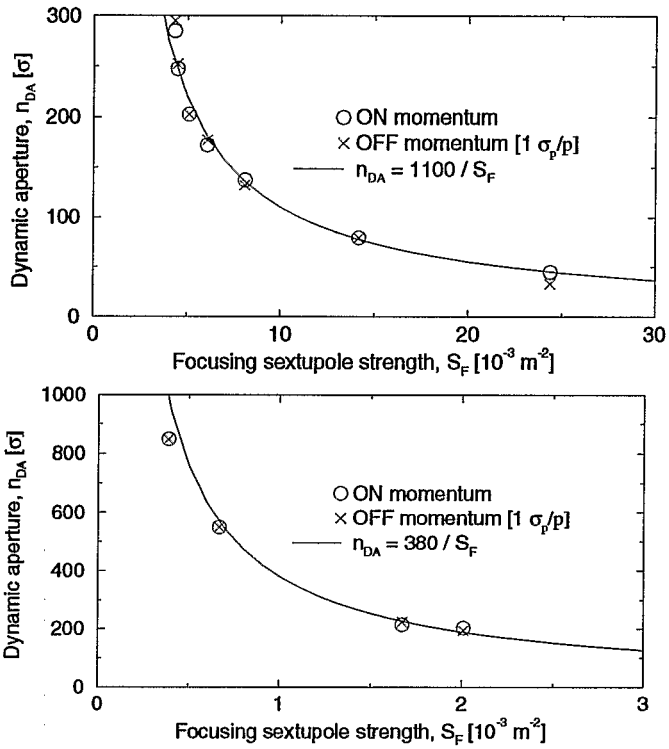

Figure 4: Dynamic aperture (10^4 turns) in the SHORT lattice (top) and the LONG lattice (bottom).

VI. REFERENCES

[1] *Proceedings of the Workshop on Future Hadron Facilities in the US*, Bloomington, FERMILAB-TM-1907, 1994.

[2] M. J. Syphers et al, Dallas, PAC Proc., 1995, p. 431

[3] *A Proposal to Conduct an Investigation into High T_c Materials for Superconducting Magnets for Next Generation Accelerators*, M. Harrison et al, Brookhaven, unpub., 1996

[4] *Accelerator Physics Issues for a Superconducting Super Collider*, Ann Arbor, UM HE 84-1, 1984

[5] *Feedback between Accelerator Physicists and Magnet Builders*, S. Peggs, Montreux 1995, Proc. to be published in Part. Acc. (also RHIC note RHIC/AP/80), 1996

[6] *Estimating and Adjusting Field Quality in Superconducting Magnets*, R. Gupta, Montreux 1995, Proc. to be published in Part. Acc. (also RHIC note RHIC/AP/87), 1996

[7] S. Peggs, Novosibirsk, Proc. 13th Int. Conf. on H. E. Accelerators, (also SSC note SSC-85), 1986

[8] S. Peck, Snowmass, Proc. SSC Summer Study, 1984, p. 384

[9] *Tolerable Systematic Errors in Really Large Hadron Collider Dipoles*, S. Peggs and F. Dell, these proceedings, 1996.

TOLERABLE SYSTEMATIC ERRORS IN REALLY LARGE HADRON COLLIDER DIPOLES

S. Peggs, F. Dell, Brookhaven National Laboratory

ABSTRACT

Maximum allowable systematic harmonics for arc dipoles in a Really Large Hadron Collider are derived. The possibility of half cell lengths much greater than 100 meters is justified. A convenient analytical model evaluating horizontal tune shifts is developed, and tested against a sample high field collider.

I. INTRODUCTION

Both "low field" and "high field" concepts of a future Really Large Hadron Collider (RLHC) were discussed at Snowmass 96. Both concepts invoke novel magnet designs. The goal of this paper is to establish semi-quantitative estimates of what would constitute good or bad field quality in arc dipoles in either machine, and to directly draw the connection between field quality and maximum (optimum) half cell length. It is implicitly assumed (after the discussion immediately below) that systematic errors dominate random errors, and that they therefore deserve the closest attention. It is fortunate that this appears to be true for contemporary superconducting magnets - if not for future magnets using high temperature superconductor technology - since it is far harder to make even semi-quantitative mathematical statements about random errors.

A. Do systematic or random errors dominate?

In 1983, when the Ann Arbor SSC workshop was held, the SSC was little more than a gleam in the physicists eye. The proceedings of that workshop contain the first systematically documented attempts to predict SSC dipole harmonic errors [1]. These predictions rested heavily on extrapolations from the limited experience with superconducting magnets then available - from the Tevatron and Isabelle/CBA. It was judged that, in general, *random errors were expected to dominate systematic errors* in SSC magnets. From the time that the official lattice was established in 1986 - in the Conceptual Design Report (CDR) of the SSC [2] - until the demise of the project in 1993, the SSC half cell length was consistently in the range $L_{SSC} = 100 \pm 10$ meters. The tables of expected dipole harmonic errors that were used for tracking purposes did not change significantly in this period. However, an analysis of 10 or so of the last SSC dipoles built shows that the *as built* harmonics were, in most cases, 3 to 10 times smaller than the *expected* CDR harmonics [3]. This implies that the SSC half cell length could have been much longer than 100 meters, and/or that it might have been possible to remove some of the nonlinear correctors.

Considerable experience has been gained since then, and the state of the art has been significantly advanced, with the construction of superconducting magnets for HERA-p and RHIC.

RHIC experience is that, to the contrary of the SSC canon, *systematic errors dominate random errors*. Preliminarily, it also appears that systematic errors dominate random errors in LHC magnets [4]. RHIC demonstrated that systematic harmonic errors can be adjusted during industrial production, using mil-size adjustments of mid-plane caps and coil pole shims [5]. This was done without interrupting the production line schedule - without adjusting the coil/collar/yoke geometry, and with only negligible redistribution of stress patterns. As a result, it was possible to reduce systematic harmonics in standard RHIC dipoles and quadrupoles to such an extent that the octupole and decapole correctors installed in the arcs will not be powered - except, perhaps, for the purpose of Landau damping. The only nonlinear correctors that will be powered in the arcs are two families of chromatic sextupoles.

High field quality in arc dipoles is most important at injection, when the beams are at their largest. It may therefore seem irrelevant that "tuning shims" in RHIC interaction region quadrupoles have been discovered to significantly improve top energy performance. However, the same tuning shim technology can also be used in arc dipoles at injection for the same purpose - to easily adjust several harmonics in an individual magnet *after* that magnet has been constructed and measured. Tuning shims could be used on each and every RLHC dipole magnet, to remove both systematic and random errors. Or, they could be applied to a single dipole at one end of each half cell, and a single dipole in the middle, in a "pseudo Simpson Neuffer scheme" that would correct many harmonics - at a single excitation.

B. Really Large Hadron Collider

It is fiscally imperative that RLHC designs stress simplicity, reliability, and economy - three virtues that are closely related. Complicated and copious magnet interconnects and spool pieces should be avoided wherever possible, in order to keep the average cost per meter low. One way to reduce the number of spools is to increase the half cell length as far as possible, beyond the conventional 53.4 meters of the LHC, and 100 meters of the SSC. Spool complexity can be reduced by eliminating most or all of the nonlinear correctors from the arcs. It may even be possible to correct the closed orbit and the chromaticity with sparse dipole and sextupole correctors - less than one of each per half cell [6].

The busy or disinterested reader may wish to skip the next two sections of this paper, "TUNE SHIFTS" and "MAXIMUM TUNE SHIFTS", which develop the mathematical model and demonstrate its accuracy with a high field RLHC example. It should be possible to go directly to section IV, "MAXIMUM ALLOWABLE HARMONICS", and pick up the story when it focuses on practical consequences and real numbers.

II. TUNE SHIFTS

The normal harmonic errors in a standard arc dipole are parameterized by the coefficients b_n in the expression

$$B_y = B_0 \left[1 + \sum_n \frac{b_n}{r_0^n} x_t^n \right] \quad (1)$$

where B_y is the vertical field at a horizontal displacement of x_t from the design trajectory at the center of the dipole, and r_0 is the reference radius. As a test particle moves along a dipole with a single harmonic, the horizontal angle x_t' that it makes with the design trajectory changes at the rate

$$\frac{dx_t'}{ds} = -\frac{B_0}{B\rho(1+\delta)} \frac{b_n}{r_0^n} x_t^n \quad (2)$$

where $B\rho$ is the on-momentum magnetic rigidity and $\delta = \Delta p/p$ is the relative momentum offset. Assuming a perfect closed orbit, the total horizontal displacement is given by

$$x_t = x + \eta\delta \quad (3)$$
$$x = A_x \cos(\phi_x) \quad (4)$$

where x is the betatron displacement contribution, A_x and ϕ_x are the betatron amplitude and phase, and η is the dispersion function at that location. The rate of change of betatron angle is derived from Equation 2, after recognizing that the dispersion itself is modified by the error harmonic. This gives

$$\frac{dx'}{ds} = -\frac{B_0}{B\rho(1+\delta)} \frac{b_n}{r_0^n} \left[(x+\eta\delta)^n - (\eta\delta)^n \right] \quad (5)$$

To proceed to calculate the horizontal tune shift as a function of A_x and δ, it is next necessary to derive the additional betatron phase advance as dipoles are traversed.

Consider a single discrete angular kick $\delta x'$. The additional betatron phase advance is given by

$$\delta\phi_x = -\frac{\beta_x \cos\phi_x}{A_x} \delta x' \quad (6)$$

where β_x is the horizontal beta function at that location. The total betatron phase advance in one turn, number n, is therefore given by an integral over all dipoles

$$\Delta\phi_x(n) = -\int_{dip} \frac{\beta_x \cos\phi_x}{A_x} \frac{dx'}{ds} ds \quad (7)$$

The one turn phase advance fluctuates from turn to turn, since it depends on the initial betatron phase at the beginning of the turn, while the betatron tune shift ΔQ_x is found by averaging the phase advance over many turns. That is,

$$\Delta Q_x = \frac{\langle \Delta\phi_x \rangle}{2\pi} \quad (8)$$

where the angle brackets denote an average over many turns, or equivalently (it is assumed), an average over the initial betatron phase. Putting all this together,

$$\Delta Q_x = \frac{b_n}{r_0^n(1+\delta)} \left\langle \frac{\beta_x \cos\phi_x}{A_x} \left(A_x \cos(\phi_x) + \eta\delta \right)^n \right\rangle \quad (9)$$

where the facts that

$$\int_{dip} \frac{B_0}{B\rho} ds \equiv 2\pi \quad (10)$$

and

$$\left\langle \frac{\beta_x \cos\phi_x}{A_x} (\eta\delta)^n \right\rangle = 0 \quad (11)$$

have been used. Angle brackets now denote a double average, over all the dipoles in the lattice and over the betatron phase.

The tune shift is a function of the betatron amplitude and the (constant) momentum offset, which are conveniently parameterized by m_x and m_δ in writing

$$A_x = m_x \sigma_x \quad (12)$$
$$\eta\delta = m_\delta \sigma_\delta \quad (13)$$

where the root mean square betatron and momentum beam sizes are

$$\sigma_x = \sqrt{\frac{\epsilon_x \beta_x}{(\beta\gamma)}} \quad (14)$$
$$\sigma_\delta = \eta \frac{\sigma_p}{p} \quad (15)$$

Here ϵ_x is the horizontal normalized emittance, and σ_p/p is the RMS relative momentum spread.

A. Master equation

This allows the master equation to be written as

$$\Delta Q_x = \frac{b_n}{r_0^n(1+\delta)} \sum_{i=0}^{n-1-2i\geq 0} C_{n,i} A_{n,i} m_\delta^{n-1-2i} m_x^{2i} \quad (16)$$

where $A_{n,i}$ are optical averages over dipoles

$$A_{n,i} = \langle \beta_x \sigma_\delta^{n-1-2i} \sigma_x^{2i} \rangle \quad (17)$$

and $C_{n,i}$ are constant coefficients

$$C_{n,i} = \frac{1}{2^{2i+1}} \frac{n!(2i+2)!}{(n-2i-1)!(2i+1)!(i+1)!(i+1)!} \quad (18)$$

These coefficients result from betatron phase averages of $\cos^m(\phi)$ terms, multiplied by binomial coefficients generated when Equation 9 is expanded into a polynomial series. Their values, up to 14-pole, are displayed in Table I.

For illustration purposes, consider a simple lattice with a single short dipole in the middle of each half cell. The optical averages depend only on optical function values at the dipole. Tune shifts for different harmonic errors are given in Table II.

B. Scaling with cell length, emittance, and energy

The optical averages $A_{n,i}$ depend on the lattice, the emittance, the momentum spread, and the energy. To see how the tune shift scales, assume that there is a standard FODO cell in the arcs, with a phase advance per cell of ϕ_c. It is also necessary to

Table I: $C_{n,i}$ coefficients for harmonics up to 14-pole.

n	Multipole	$i=0$	1	2
1	Quadrupole	1/2		
2	Sextupole	1		
3	Octupole	3/2	3/8	
4	Decapole	2	3/2	
5	12-pole	5/2	15/4	5/16
6	14-pole	3	15/2	15/8

Table II: Tune shifts for the simple example of one thin dipole in the middle of each half cell. $b'_n = b_n/(1+\delta)$.

Multipole	ΔQ_x
Quadrupole	$b'_1\beta_x\frac{1}{2}$
Sextupole	$b'_2\beta_x(\eta\delta)$
Octupole	$b'_3\beta_x[3/2(\eta\delta)^2 + 3/8A_x^2]$
Decapole	$b'_4\beta_x[2(\eta\delta)^3 + 3/2(\eta\delta)A_x^2]$
12-pole	$b'_5\beta_x[5/2(\eta\delta)^4 + 15/4(\eta\delta)^2A_x^2 + 5/16A_x^4]$
14-pole	$b'_6\beta_x[3(\eta\delta)^5 + 15/2(\eta\delta)^3A_x^2 + 15/8(\eta\delta)A_x^4]$

assume some relationship between the betatron and momentum contributions to the total horizontal beam size. For example, suppose that the RMS momentum spread is manipulated with a fixed longitudinal emittance by adjusting the RF voltage, so that the two contributions are equal where they are largest

$$\widehat{\sigma_\delta} = \widehat{\sigma_x} \tag{19}$$

at the center of the horizontally focusing quadrupole. This is physically reasonable for a high field 30 TeV hadron collider [7]. It is then easy to show that

$$A_{n,i} = \alpha_{n,i}(\phi_c)\, L^{(n+1)/2} \left(\frac{\epsilon_x}{\beta\gamma}\right)^{(n-1)/2} \tag{20}$$

where L is the half cell length, and $\alpha_{n,i}$ is a non-trivial function of (only) the phase advance per cell. This makes it possible (finally!) to write down how the tune shift scales with cell length, emittance, and energy. Substituting Equation 20 into the master equation, Equation 16, gives

$$\Delta Q_x = \frac{b_n}{r_0^n(1+\delta)} L^{(n+1)/2} \left(\frac{\epsilon_x}{\beta\gamma}\right)^{(n-1)/2} \times \sum_{i=0}^{n-1-2i\geq 0} C_{n,i}\alpha_{n,i}(\phi_c)\, m_\delta^{n-1-2i}\, m_x^{2i} \tag{21}$$

This relatively ugly expression has the virtue of laying bare the dependence of the tune shift on all the parameters of interest.

Table III lists the $\alpha_{n,i}$ values for a lattice with thin quadrupoles in which the FODO cells are fully packed with dipoles - a fair approximation for an RLHC - with a 90 degree phase advance per cell. The application of Tables I and III to Equation 21 is then straightforward, if messy.

Table III: Numerically calculated values for $\alpha_{n,i}$ for fully packed FODO cells with $\phi_c = 90$ degrees per cell.

n	Multipole	$i=0$	1	2
1	Quadrupole	1.667		
2	Sextupole	2.412		
3	Octupole	3.608	3.467	
4	Decapole	5.555	5.381	
5	12-pole	8.753	8.536	8.340
6	14-pole	14.06	13.78	13.53

III. MAXIMUM TUNE SHIFTS

A numerical study of two high field RLHC designs has been performed, in order to verify the accuracy of the mathematical model, and to establish an approximate value for the maximum tolerable horizontal tune shift. Tables IV and V summarize the common primary parameters, and the different lattice parameters, for SHORT and LONG cell high field machines that are described in more detail elsewhere in these proceedings [7].

A. Tracking results

Figure 1 shows the tune shift versus momentum in the SHORT machine for various values of m_x, with a systematic octupole harmonic of $b_3 = 5 \times 10^{-4}$ in the top plot, and a de-

Table IV: Primary parameters for a high field RLHC.

Parameter	units	value
Storage energy	[TeV]	30.0
Injection energy	[TeV]	1.0
Dipole field (store)	[T]	12.5
Dipole coil ID	[mm]	50 - 60
Transverse RMS emittance, ϵ	[μm]	1.0

Table V: Lattice parameters for SHORT and LONG cell high field machines, at injection.

Parameter	units	SHORT	LONG
Half cell length, L	[m]	110	260
Max. cell beta, $\widehat{\beta}$	[m]	376	898
Max. cell dispersion, $\widehat{\eta}$	[m]	3.85	22.9
Max. betatron size, $\widehat{\sigma}_\beta$	[mm]	.594	.918
Circumference, C	[km]	55.44	54.08
Horizontal tune, Q_x		65.195	28.195
Vertical tune, Q_y		66.185	29.185
Number of dipoles		2888	2900
Number of sextupoles		456	168
Mmtm. width, σ_p/p	[10^{-3}]	.1545	.0401

capole systematic of $b_4 = 30 \times 10^{-4}$ in the bottom plot. A reference radius of $r_0 = 16$ mm is used throughout. Solid lines in the figure show the predictions of the model developed above, while data points represent the tune shifts measured using the tracking code TEAPOT.

The most striking general feature of these plots is that a systematic octupole (decapole) harmonic generates curves with an even (odd) symmetry. Agreement between prediction and measurement is quite good at small m_x and small m_δ, but not perfect. This discrepancy is mostly due to the presence of dispersion supressors, and the fact that the dipole packing fraction is only 81.8%, and not the 100% assumed in the model. Both of these factors throw the predicted optical averages $A_{n,i}$ into error. The packing fraction in the LONG machine is 86.5%, leading to a significant reduction of the total circumference by 1.36 km, or 2.5%.

The horizontal base tune was lowered to $Q_x = 65.145$ for this exercise, in order to place it approximately midway between the integer and fourth order resonances at 65.0 and 65.25, respectively. In principle, a perfectly smoothly distributed systematic octupole harmonic does not drive the fourth order resonance, due to vector cancellation. In practice, the cancellation is not perfect, and so the top plot clearly saturates at a tune shift of approximately $+0.1$, when the fourth order resonance is approached. The bottom plot shows minimum tune shifts of approximately -0.1, when the integer resonance is approached.

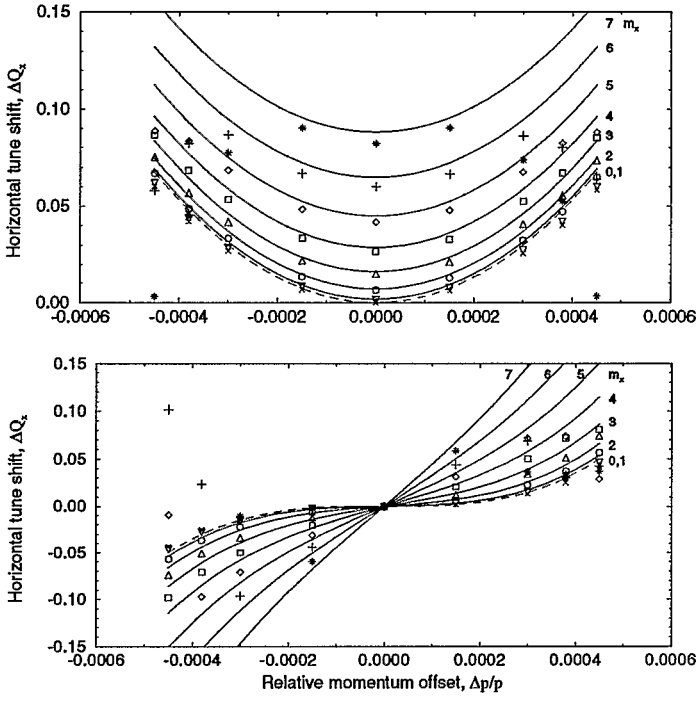

Figure 1: Tune shifts due to systematic octupole (top) and decapole (bottom) harmonics in SHORT machine dipoles. Solid lines are predictions, while data points are measured results.

It is entirely within the semi-quantitative spirit of this paper that the model and the analysis only discuss 1-D motion, in the horizontal. A more rigorous discussion would also include vertical betatron motion - and would also include synchrotron oscillations, and a whole host of realistic effects. As RLHC designs become more refined, so too must the simulations. At this point, when the RLHC is hardly even a gleam in the physicists eye, clarity and simplicity are more important than rigor.

IV. MAXIMUM ALLOWABLE HARMONICS

While the previous section focused on the particular example of a 30 TeV high field collider, the conclusion that the maximum tolerable tune shift is

$$\widehat{\Delta Q_x} \approx 0.1 \tag{22}$$

is expected to hold in general - for any low or high field collider, at low or high energy, that conforms with the physical assumptions made so far:
1) systematic errors dominate random errors
2) the collider has many fully packed FODO cells
3) momentum and betatron beam sizes at F quads are equal
4) $\phi_c = 90$ degrees phase advance per cell
5) chromaticity sextupoles are not pathologically strong
It is relatively straightforward to derive the semi-quantitative results, below, for phase advances per cell other than 90 degrees. For example, while maximum allowable harmonics are smaller at 60 degrees per cell, there is not much advantage in increasing ϕ_c beyond 90 degrees per cell.

What is the necessary field quality in such a machine? How large can the half cell length L be? Suppose, for example, that the horizontal tune shift must be guaranteed to be less than $\widehat{\Delta Q_x}$ for all test particles in the betatron amplitude and momentum distribution range

$$m_x \leq m \tag{23}$$
$$|m_\delta| \leq m \tag{24}$$

The extreme tune shift occurs when $m_x = m_\delta = m$, and is given by

$$\Delta Q_x(m) = \frac{b_n}{r_0^n} D_n \, m^{n-1} \, L^{(n+1)/2} \left(\frac{\epsilon_x}{\beta\gamma}\right)^{(n-1)/2} \tag{25}$$

An irritating and negligible term $(1+\delta)$ has been unceremoniously dropped from the denominator of this equation, in order to make it as simple as possible in comparison with the more general result of Equation 21, from which it is derived. The sum in Equation 21 has been replaced by D_n, a function of the phase advance per cell, which is given by

$$D_n(\phi_c) = \sum_{i=0}^{n-1-2i\geq 0} C_{n,i} \, \alpha_{n,i}(\phi_c) \tag{26}$$

Numerical values for D_n, derived from Tables I and III, are listed in Table VI.

Table VI: Lowest order D_n values, with a phase advance of $\phi_c = 90$ degrees per FODO cell.

n	Multipole	D_n
1	Quadrupole	.8333
2	Sextupole	2.412
3	Octupole	6.712
4	Decapole	19.18
5	12-pole	56.49
6	14-pole	170.9

Equation 25 is readily inverted, to give the maximum allowed systematic harmonic

$$\frac{b_n}{r_0^n} \leq \widehat{\Delta Q_x} \frac{1}{D_n} L^{-(n+1)/2} \left(\frac{\beta\gamma}{m^2 \epsilon_x} \right)^{(n-1)/2} \qquad (27)$$

For example, with $\Delta Q_x(m) = \widehat{\Delta Q_x} = 0.1$, an injection energy of 1 TeV, $\epsilon_x = 1$ micron, and defining the edge of the particle distribution of interest by $m = 3$, then the maximum systematic harmonics are plotted for octupole through 14-pole harmonics in Figure 2. The lowest allowed harmonic, sextupole, is not shown in the Figure, since chromatic sextupoles are naturally available to correct b_2, and a proper analysis of its maximum tolerable value goes beyond the scope of this paper. The harmonics of most concern are the unallowed octupole b_3, which has the tightest tolerances but which is naturally relatively small, and the allowed decapole b_4, which is probably the most critical harmonic in practice.

It is worth inspecting the scaling in Equation 27 with a critical eye. The allowable systematic errors increase rapidly as the injection energy is increased - from 1 TeV to 3 TeV, for example - and as the injection emittance is decreased. Similarly, the chosen value of m is very important, and needs more discussion than the simple assertion, in this paper, that a value of $m = 3$ is reasonable.

V. CONCLUSIONS

Lattices with relatively long arc cells have potential advantages, including significant cost savings, in a Really Large Hadron Collider. However, the susceptibility of the beam dynamics to systematic arc dipole errors increases as the cell gets longer. Therefore, reasonable expectations for the achievable dipole field quality at injection play a strong role in determining the cell length - or vice versa.

For example, if beam with a normalized emittance of 1 micron is injected at 1 TeV into a lattice with half cells $L = 300$ meters long, then dipoles with a systematic decapole of $b_4 \simeq 3 \times 10^{-4}$ (at a reference radius of 16 mm) will provide barely adequate performance. Higher values of this allowed harmonic would increase the horizontal tune shift beyond the rule-of-thumb physical maximum of $\widehat{\Delta Q_x} \approx 0.1$. The systematic tolerance at the same half cell length for the next allowed harmonic, the 14-pole, is $b_6 \simeq 30 \times 10^{-4}$. For the unallowed octupole and 12-pole harmonics the equivalent tolerances are $b_3 \simeq 0.8 \times 10^{-4}$ and $b_5 \simeq 10 \times 10^{-4}$, respectively.

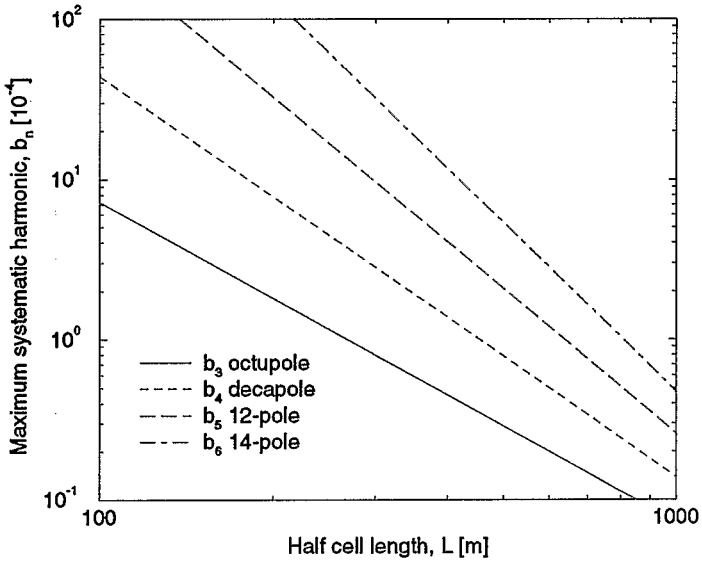

Figure 2: Maximum allowable systematic harmonics versus half cell length, when $\widehat{\Delta Q_x} = 0.1$, $\epsilon_x = 1$ micron, and $m = 3$, at an energy of 1 TeV.

Future hadron colliders with half cell lengths of a few hundred meters are cost effective, with adequate beam dynamics performance. This is especially true for high field colliders, in which the radiation damping forgivingly allows less stringent field quality tolerances.

VI. REFERENCES

[1] *Accelerator Physics Issues for a Superconducting Super Collider*, Ann Arbor, UM HE 84-1, 1984. See the working group reports by R. Talman (p. 28), and R. Palmer (p. 32), and the individual papers by E. Bleser et al, D. Douglas, H.E. Fisk, R. Meuser, and S. Ohnuma (pp. 95, 96, 119, 132, 147).

[2] *Conceptual Design*, SSC Central Design Group, Berkeley, SSC-SR-2020, 1986.

[3] *Estimating and Adjusting Field Quality in Superconducting Magnets*, R. Gupta, Montreux 1995, Proc. to be published in Part. Acc. (also RHIC note RHIC/AP/87), 1996

[4] private communications with Frank Schmidt, 1996.

[5] *Feedback between Accelerator Physicists and Magnet Builders*, S. Peggs, Montreux 1995, Proc. to be published in Part. Acc. (also RHIC note RHIC/AP/80), 1996

[6] *Proceedings of the Workshop on Future Hadron Facilities in the US*, Bloomington, FERMILAB-TM-1907, 1994.

[7] *Lattices for a High-Field 30 TeV Hadron Collider*, S. Peggs et al, these proceedings, 1996.